

## Article

# The Effect of Ge Doping on $\alpha$ -Ag<sub>2</sub>S's Thermoelectric and Mechanical Properties

Gabriela Hrickova <sup>1,\*</sup>, Frantisek Mihok <sup>2</sup>, Zuzana Molcanova <sup>3</sup>, Beata Ballokova <sup>3</sup>, Wanda Mamrilla <sup>4</sup>, Robert Dzunda <sup>3</sup>, Peter Lukacs <sup>1</sup>, Alena Pietrikova <sup>1</sup> and Karel Saksl <sup>2</sup>

<sup>1</sup> Department of Technologies in Electronics, Faculty of Electrical Engineering and Informatics, Technical University of Kosice, 04001 Kosice, Slovakia; peter.lukacs@tuke.sk (P.L.); alena.pietrikova@tuke.sk (A.P.)

<sup>2</sup> Faculty of Materials, Metallurgy and Recycling, Technical University of Kosice, 04001 Kosice, Slovakia; fmihok@saske.sk (F.M.); karel.saksl@tuke.sk (K.S.)

<sup>3</sup> Institute of Materials Research, Slovak Academy of Science Kosice, 04001 Kosice, Slovakia; molcanova@saske.sk (Z.M.); bballokova@saske.sk (B.B.); rdzunda@saske.sk (R.D.)

<sup>4</sup> Department of Biomedical Engineering and Measurement, Faculty of Mechanical Engineering, Technical University of Kosice, 04001 Kosice, Slovakia; wanda.mamrilla@tuke.sk

\* Correspondence: gabriela.hrickova@tuke.sk; Tel.: +421-55-6023199

**Abstract:** Thermoelectric materials are capable of generating electrical energy in response to a temperature gradient. Non-renewable energy resources are depleting, so the development of renewable energy sources that are environmentally sustainable is essential. One potential application of these materials as an alternative energy source is in wearable electronics. Thermoelectric materials are used in common electrical devices, as well as by the military, in healthcare, and in space. As a ductile N-type semiconducting material, silver sulfide is one of the most promising materials in terms of thermoelectric potential. The properties of Ag<sub>2</sub>S can be improved by choosing the appropriate dopants. This study investigates the methods by which the thermoelectric, mechanical, and hardness properties of Ag<sub>2</sub>S are improved via Ge doping. The addition of Ge increases the Seebeck coefficient to a maximum of  $-87 \mu\text{V}\cdot\text{K}^{-1}$  from  $-1051 \mu\text{V}\cdot\text{K}^{-1}$  to P-type, bringing it closer to transitioning. In order to work, a thermoelectric generator requires both N- and P-type materials. By applying homo-junctions made from similar materials, internal stresses caused by the varying thermal expansion rates of different materials are reduced. In order to demonstrate Ge integration, scanning electron microscopy and X-ray diffraction were applied to the sample microstructure. In addition, supplementation was used to increase the ductility and malleability of materials to make them suitable for power generation in wearable electronics. These materials showed significant power factor values according to room-temperature measurements. This proves that materials capable of generating usable voltage lie in the recommended ambient temperature range for the user's body, thus rendering them potential candidates for wearable electronics.

**Keywords:** Ag<sub>2</sub>S; thermoelectric; wearable electronics



**Citation:** Hrickova, G.; Mihok, F.; Molcanova, Z.; Ballokova, B.; Mamrilla, W.; Dzunda, R.; Lukacs, P.; Pietrikova, A.; Saksl, K. The Effect of Ge Doping on  $\alpha$ -Ag<sub>2</sub>S's Thermoelectric and Mechanical Properties. *Inorganics* **2024**, *12*, 98. <https://doi.org/10.3390/inorganics12040098>

Academic Editor: Jean-François Halet

Received: 1 February 2024

Revised: 14 March 2024

Accepted: 25 March 2024

Published: 28 March 2024



**Copyright:** © 2024 by the authors. Licensee MDPI, Basel, Switzerland. This article is an open access article distributed under the terms and conditions of the Creative Commons Attribution (CC BY) license (<https://creativecommons.org/licenses/by/4.0/>).

## 1. Introduction

In a thermoelectric material, the thermoelectric effect is the immediate transformation of a temperature difference into electric voltage, or vice versa. An electric voltage is generated by thermoelectric materials when the temperatures at their extremities differ. Furthermore, this phenomenon exhibits reversibility; that is, the application of electric voltage to the opposite extremities of a thermoelectric material causes heat transfer, thereby generating a disparity and a temperature gradient between those extremities. Substrates, and electrically conductive materials in general, exhibit thermoelectric effects. The Seebeck effect, the Peltier effect, and the Thomson effect are the three main thermoelectric effects [1–3]. Over the course of the last decade, numerous industrial, medical, space, and

military applications have been built upon thermoelectric effects [4–7]. Lead and chalcogenides (PbX, X = S, Se, Te;  $zT_{\text{MAX}} = 2.1$ ), bismuth telluride ( $zT_{\text{MAX}} = 1.4$ ) [4], SiGe alloys ( $zT_{\text{MAX}} < 1$ ) [8], Zintl phases ( $zT_{\text{MAX}} < 1.3$ ) [9], half-Heusler alloys ( $zT_{\text{MAX}} = 1.52$ ) [10], and organic thermoelectrics ( $zT_{\text{MAX}} < 0.42$ ) [11] are a few of the previously developed thermoelectric alloys. Environmental friendliness, quiet operation, durability, dependability, resistance to wear, and the absence of moving parts are the primary benefits of thermoelectric devices. Thermoelectric devices are easily manipulated and exhibit an immediate response to changes in power requirements. In general, thermoelectric devices fall into two classifications: those used for power generation, cooling, or heating, and those designated for temperature measurement ( $zT \approx 10^{-6}$ – $10^{-3}$ ). The Peltier and Seebeck effects are utilized by the majority of thermoelectric refrigerators and generators, respectively [1,12–14]. Thermoelectric cooling devices that are commercially available find application in a wide range of fields and sectors, such as aerospace, consumer products, laboratory and scientific devices, industrial temperature regulation, and restaurant equipment, among others [12–18].

The Peltier effect is a phenomenon wherein the injection of an electric current in a material (or two different materials) produces a temperature gradient. By utilizing this temperature difference, an object can be either heated or cooled. If a temperature difference exists between the hot and cold extremities of a thermoelectric device, it can operate as an electric power generator [15,19]. Wearable electronics, such as smart glasses, jewelry, and wristwatches, represent a viable domain in which flexible thermoelectric generators can be effectively utilized. These devices are capable of converting waste energy from the human body into electrical energy essential for charging wearable devices.

Given the impending depletion of specific energy sources and environmental concerns, as well as the possibility of an energy crisis, it is expected that these electronics will find substantial utility in the future [4,18–23]. As a result, attention must be focused on alternative energy sources, including thermoelectric devices.

Due to its ductile characteristics [24–27], Ag<sub>2</sub>S demonstrates significant promise as a material suitable for integration into flexible thermoelectric generators; thus, it can serve as the foundation for thermoelectric devices that will experience mechanical stresses. Ag<sub>2</sub>S is also polymorphic, which signifies that its crystal structure alters with increasing temperature [28–31]. Acanthite is a naturally occurring mineral composed of monoclinic  $\alpha$ -Ag<sub>2</sub>S.  $\alpha$ -Ag<sub>2</sub>S is present at temperatures below 177 °C. A phase transition occurs from a monoclinic crystal structure to a body-centered cubic  $\beta$ -Ag<sub>2</sub>S when the temperature surpasses 177 °C.  $\beta$ -Ag<sub>2</sub>S is naturally present in the form of the mineral argentite at temperatures ranging from 177 °C to 592 °C. The final crystal modification of Ag<sub>2</sub>S is  $\gamma$ -Ag<sub>2</sub>S, a mineral with a cubic face-centered crystal structure. The temperature range of  $\gamma$ -Ag<sub>2</sub>S spans from 592 °C to 837 °C, which corresponds to its melting point [32]. At ambient temperature, monoclinic  $\alpha$ -Ag<sub>2</sub>S exhibits the following properties as an N-type non-degenerate semiconductor: a low electron concentration of  $1.6 \times 10^{14} \text{ cm}^{-3}$ , a high negative Seebeck coefficient of  $-1051 \mu\text{V}\cdot\text{K}^{-1}$ , a low electrical conductivity  $\sigma$  ranging from 0.09 to  $0.16 \text{ S}\cdot\text{m}^{-1}$ , and a low thermal conductivity  $\kappa$   $0.5 \text{ W}\cdot\text{m}^{-1}\cdot\text{K}^{-1}$  [27,30,33,34]. Pure  $\alpha$ -Ag<sub>2</sub>S is deemed unsuitable for use as a thermoelectric material due to its negligible  $zT$  value ( $\approx 0$ ), which limits its effective application, in the absence of impurities. Significant improvement in its thermoelectric properties can be achieved through doping with an appropriate chalcogen or metalloid. Se and Te are the chalcogens that have the potential to improve the thermoelectric characteristics of Ag<sub>2</sub>S. An additional category of elements that can substitute for S in Ag<sub>2</sub>S is metalloids. Suitable metalloids, with the exception of Te, comprise the subsequent elements: B, Si, Ge, As, and Sb. Pure elements, including Te, Se, Sb, and Ge, have been proposed to be capable of occupying the S positions in the Ag<sub>2</sub>S compound [2,26,35].

A study has shown the effective synthesis of non- $\alpha$  Ag<sub>2</sub>S thermoelectric materials doped with Se and Te (with Te serving as a substitute for S) [36]. Nevertheless, our goal

was to analyze Ge-doped  $\alpha$ -Ag<sub>2</sub>S material using a monoclinic unit cell in order to produce a P-type material, preferably with minimal doping.

The power factor PF and the figure of merit  $zT$  are the two most significant thermoelectric parameters that characterize a thermoelectric material. The figure of merit ( $zT$ ), which indicates the thermoelectric efficiency of a material, is defined as follows:

$$zT = \frac{\alpha^2 \cdot \sigma}{\kappa} \cdot T, \quad (1)$$

where  $\alpha$  represents the Seebeck coefficient,  $\sigma$  represents the electrical conductivity,  $\kappa$  represents the thermal conductivity, and  $T$  is the thermodynamic temperature [8,11,25,37–41]. Thermoelectric materials that are used for heat transfer or electricity generation generally possess  $zT$  values not exceeding 1 and  $PF = \alpha^2 \cdot \sigma$  values starting from tens of  $\mu\text{W} \cdot \text{cm}^{-1} \cdot \text{K}^{-2}$ . Therefore, for a material to be considered effectively thermoelectric, it is essential that it possesses the maximum power generation/conversion efficiency ( $zT$ ). This is achieved by specifying large values for  $\sigma$  and  $\alpha$ , while maintaining a low value for  $\kappa$  [2].

## 2. Results

### 2.1. Chemical Composition and Electron Microscopy Analysis of the Microstructure

A local scanning electron microscopy with energy dispersive X-ray spectroscopy SEM EDX point analysis was carried out on a 1 mm by 1 mm area for each sample. The elemental content (Ag, S, Ge) values for each sample, predicted and measured through EDX, are presented in Table 1 and Figure 1. The known cause for the discrepancies observed in the powder mixtures is the inadequate homogenization of the constituent elements or powders.

**Table 1.** Chemical composition of the analyzed materials.

Expected Composition	Ag <sub>2</sub> S	Ag <sub>2</sub> Ge <sub>0.05</sub> S <sub>0.95</sub>	Ag <sub>2</sub> Ge <sub>0.1</sub> S <sub>0.9</sub>	Ag <sub>2</sub> Ge <sub>0.2</sub> S <sub>0.8</sub>	Ag <sub>2</sub> Ge <sub>0.3</sub> S <sub>0.7</sub>	
Measured	Ag (at.%)	2.06	2.05	1.95	1.83	1.85
	Ge (at.%)	0	0.072	0.23	0.42	0.51
	S (at.%)	0.94	0.88	0.82	0.75	0.64

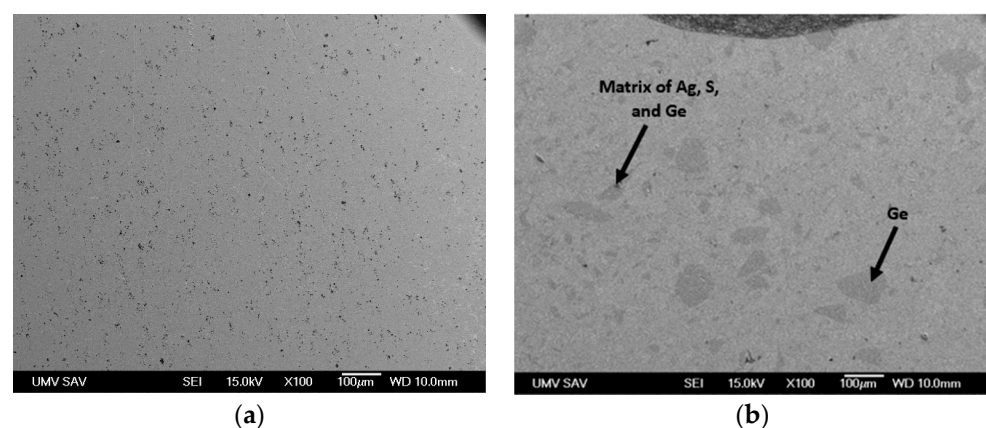


**Figure 1.** SEM images of (a) Ag<sub>2</sub>S and (b) Ag<sub>2</sub>S<sub>0.03</sub>S<sub>0.7</sub> via JEOL.

SEM (Scanning electron microscopy) cross-sections of the Ag<sub>2</sub>S and Ag<sub>2</sub>Ge<sub>0.3</sub>S<sub>0.7</sub> samples are shown in Figure 1. The annealing conditions resulted in the formation of a single crystalline phase  $\alpha$ -Ag<sub>2</sub>S from Ag and S. On the other hand, the Ag<sub>2</sub>Ge<sub>0.3</sub>S<sub>0.7</sub> sample, rich in Ge, exhibited microstructural characteristics (dark crystallites) that span a spectrum of dimensions, from nearly imperceptible particles to sizable entities exceeding 100  $\mu\text{m}$ . The crystallites consisted entirely of Ge or a compound consisting of Ag, S, and Ge. Ge segregation took place despite the inclusion of Ge particles in the initial mixture. Meanwhile, the sample matrix is defined and illustrated in Figures 2–4 as  $\alpha$ -Ag<sub>2</sub>S. Therefore, it is obvious that the Ge particles were

not completely incorporated into the  $\alpha$ -Ag<sub>2</sub>S powder through the solid-state reaction. As a result, the material could not have been adequately homogenized at 160 °C (Ge has a melting point of 938 °C). In order to obtain a more comprehensive understanding of the microstructure of the Ag<sub>2</sub>S and Ag<sub>2</sub>Ge<sub>0.3</sub>S<sub>0.7</sub> samples, 2D EDX cross-section mapping was carried out (Figures 2 and 3). Ag and S are clearly distributed uniformly in both Ag<sub>2</sub>S and Ag<sub>2</sub>Ge<sub>0.3</sub>S<sub>0.7</sub>. The exception to this rule is Ag<sub>2</sub>Ge<sub>0.3</sub>S<sub>0.7</sub>, which contains germanium sites (i.e., particles larger than 100  $\mu$ m or nearly invisible particles); these sites indicate that Ge atoms have not been incorporated into the  $\alpha$ -Ag<sub>2</sub>S unit cell, and thus Ge generates a separate crystalline phase. Ge influenced the overall characteristics of the Ag<sub>2</sub>S material by forming a small segregated area in the Ag<sub>2</sub>S matrix.

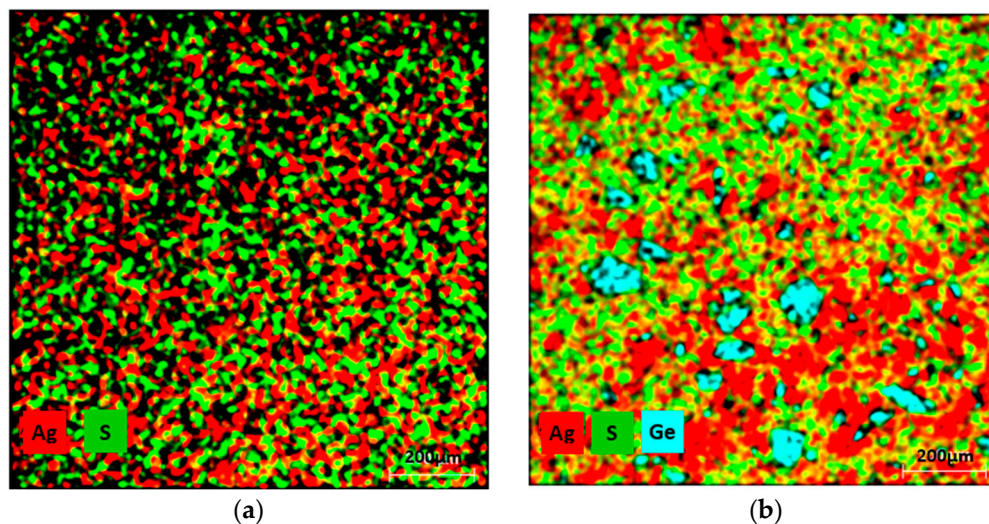


**Figure 2.** Combined elemental distribution obtained via TESCAN EDX mapping, where red represents Ag, green represents S, and turquoise represents Ge: (a) Ag<sub>2</sub>S, (b) Ag<sub>2</sub>Ge<sub>0.3</sub>S<sub>0.7</sub>.

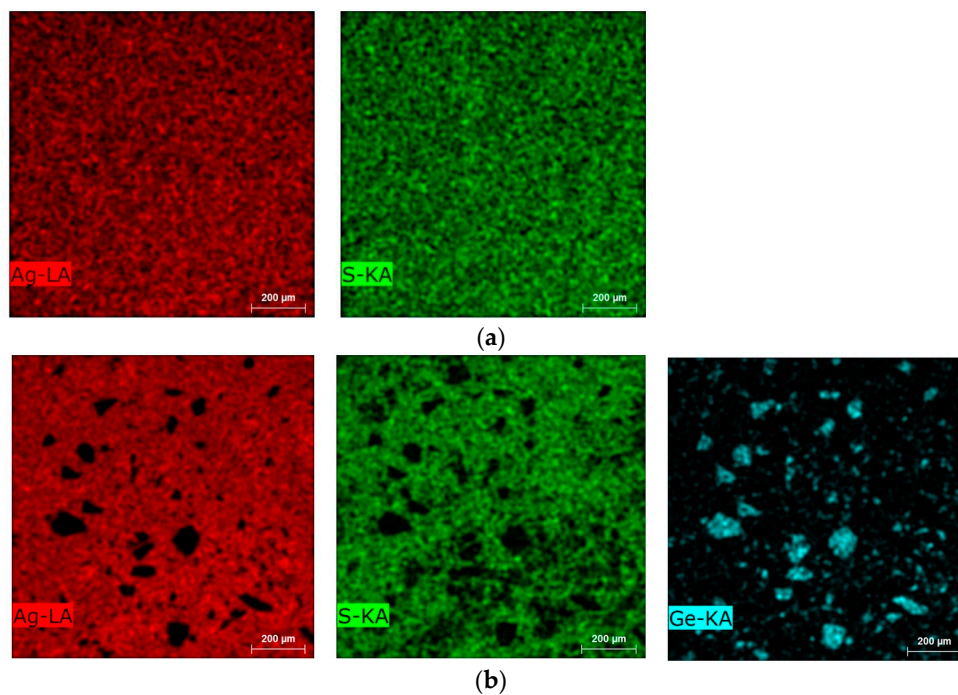


**Figure 3.** Elemental distribution via TESCAN EDX mapping: (a) Ag<sub>2</sub>S, (b) Ag<sub>2</sub>Ge<sub>0.3</sub>S<sub>0.7</sub>.

## 2.2. X-ray Diffraction Analysis of the Microstructure

The crystalline phases and unit cell parameters of the  $\alpha$ -Ag<sub>2</sub>S-based samples were determined using X-ray diffraction. Diffraction patterns were obtained at room temperature (Figure 4) within the  $2\theta$  range of 20–80°. The steps were carried out with a duration of 80 s, and a step size of  $\Delta 2\theta = 0.03^\circ$ . The crystalline nature of the samples under investigation was confirmed by the presence of Bragg peaks [42]. The diffraction data were subjected to structural analysis utilizing GSAS-II (Version 5111) software [43]. In order to determine the parameters of the  $\alpha$ -Ag<sub>2</sub>S unit cell, Rietveld refinement was applied. The unit cell parameters of  $\alpha$ -Ag<sub>2</sub>S are as follows, as reported by the Crystallography Open Database (COD):  $a = 4.229 \text{ \AA}$ ,  $b = 6.931 \text{ \AA}$ ,  $c = 7.862 \text{ \AA}$ , and  $\beta = 99.61^\circ$ . In order to enhance legibility, the observed diffraction patterns were restricted to the range of  $2\theta = 25\text{--}55^\circ$ .

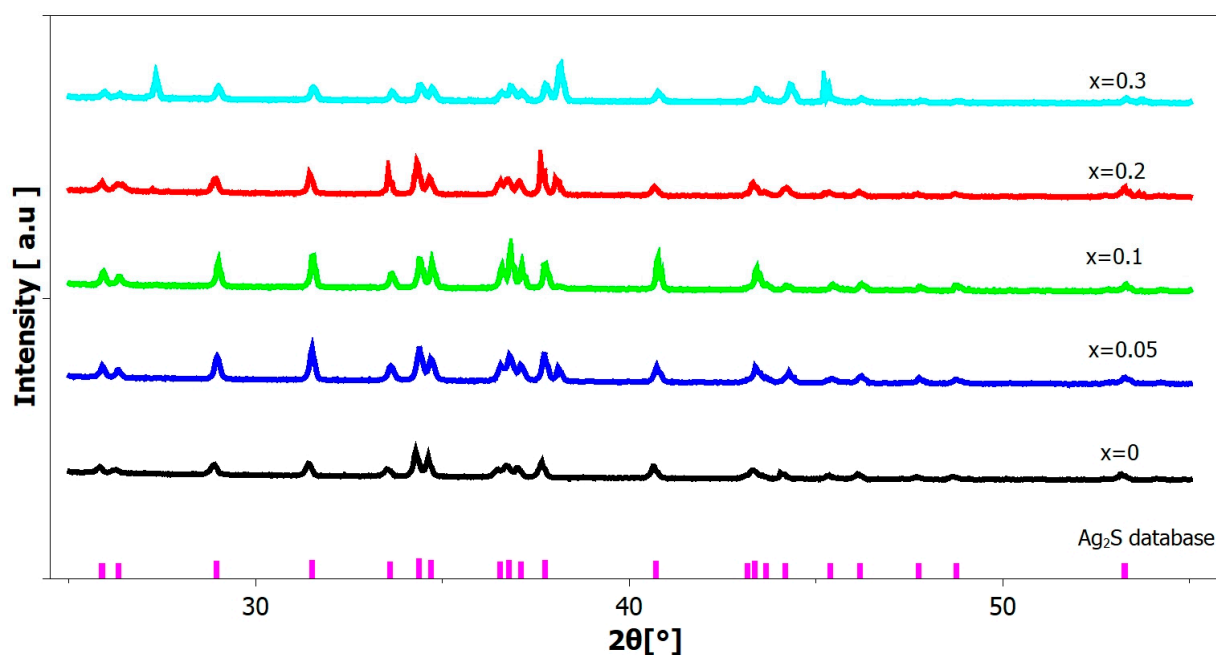


**Figure 4.** X-ray diffraction patterns of Ag<sub>2</sub>Ge<sub>x</sub>S<sub>(1-x)</sub> powder samples; purple vertical lines represent the position of diffraction peaks from the COD database [44].

The patterns show that the relative intensity of the individual Bragg peaks differed based on the sample composition. The granules under investigation contained relatively large particles ( $\alpha$ -Ag<sub>2</sub>S, Ge), which significantly contributed to the observed patterns of apparent preferred orientation. Furthermore, a variation in the concentration of the  $\alpha$ -Ag<sub>2</sub>S peaks resulting from a modification in the  $\alpha$ -Ag<sub>2</sub>S unit cell content could potentially be caused by the addition of Ge atoms into the  $\alpha$ -Ag<sub>2</sub>S unit cell. Additionally, the formation of new crystalline phases consisting of pairs, such as Ag and Ge, or S and Ge, could potentially play a role.

The Rietveld refinement of the  $\alpha$ -Ag<sub>2</sub>S crystalline phase (Figure 5) indicates that the volume of  $\alpha$ -Ag<sub>2</sub>S increased slightly with the incorporation of Ge atoms into the  $\alpha$ -Ag<sub>2</sub>S unit cell (Table 2). This resulted in an increase in the dimensions of the unit cell ( $a$ ,  $b$ , and  $c$ ). The variation in the values of  $a$ ,  $b$ , and  $c$  with respect to the Ge content of the samples can be attributed to a modification in the basic cell dimensions. The diffraction data did not reveal the presence of any additional crystalline phases, with the exception of small amounts of Ge in Ag<sub>2</sub>Ge<sub>0.3</sub>S<sub>0.7</sub> (Figure 5).

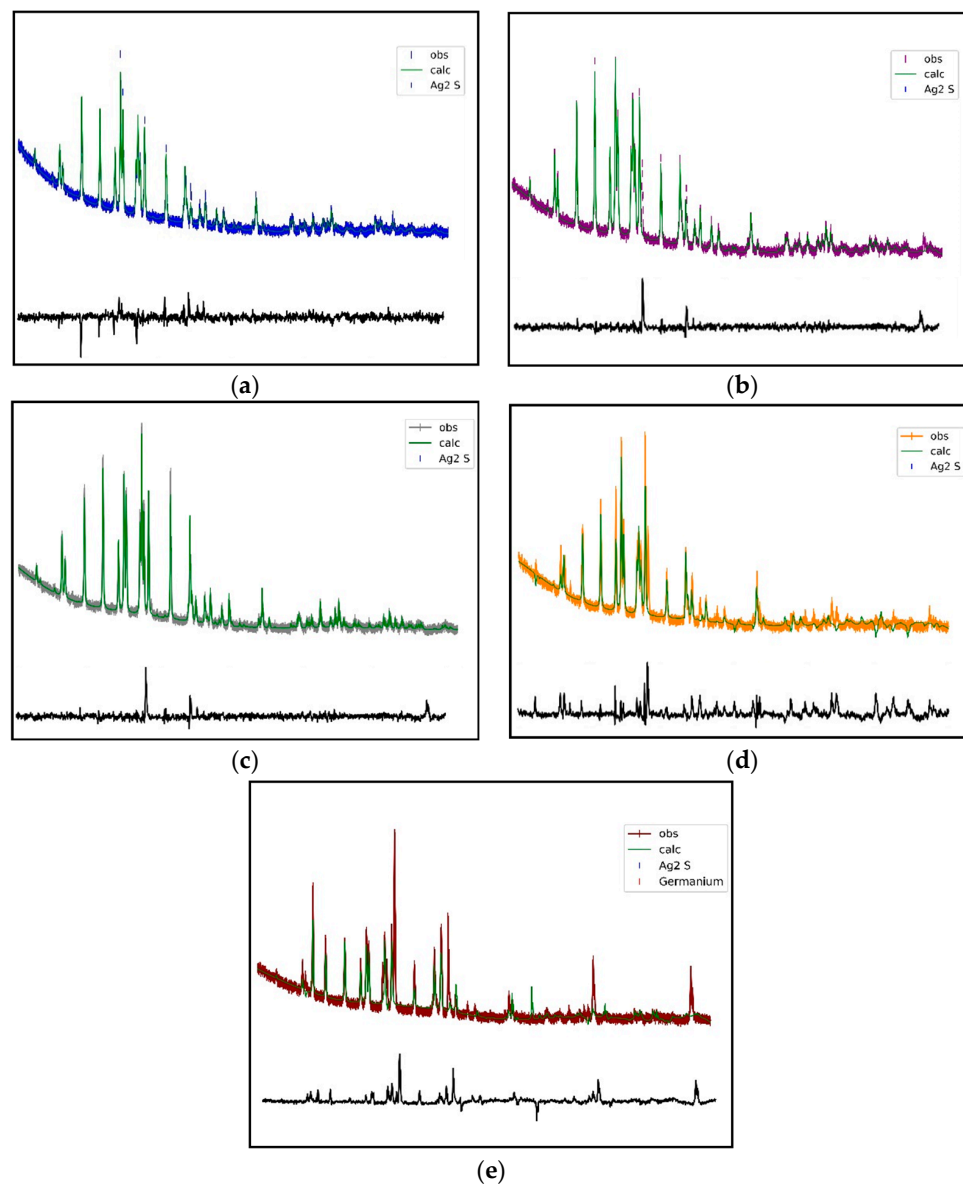


**Figure 5.** Rietveld refinement of the  $\alpha$ - $\text{Ag}_2\text{S}$  crystalline phase: (a)  $\text{Ag}_2\text{S}$ , (b)  $\text{Ag}_2\text{Ge}_{0.05}\text{S}_{0.95}$ , (c)  $\text{Ag}_2\text{Ge}_{0.1}\text{S}_{0.9}$ , (d)  $\text{Ag}_2\text{Ge}_{0.2}\text{S}_{0.8}$ , (e)  $\text{Ag}_2\text{Ge}_{0.3}\text{S}_{0.7}$ . The green line shows calculated diffraction patterns; other colored lines show observed diffraction patterns; the black line shows the difference between observed and calculated data.

**Table 2.** Parameters of the  $\alpha$ - $\text{Ag}_2\text{S}$  unit cell obtained via the Rietveld refinement of X-ray diffraction data, and the standard deviation of the parameters of the unit cell.

	a [Å]	b [Å]	c [Å]	$\beta$ [°]	Rw
$\text{Ag}_2\text{S}$	$4.228 \pm 0.001$	$6.928 \pm 0.001$	$7.864 \pm 0.002$	$99.649 \pm 0.004$	4.57
$\text{Ag}_2\text{Ge}_{0.05}\text{S}_{0.95}$	$4.225 \pm 0.001$	$6.926 \pm 0.001$	$7.862 \pm 0.002$	$99.662 \pm 0.004$	5.17
$\text{Ag}_2\text{Ge}_{0.1}\text{S}_{0.9}$	$4.228 \pm 0.0002$	$6.929 \pm 0.0002$	$7.865 \pm 0.001$	$99.652 \pm 0.002$	3.44
$\text{Ag}_2\text{Ge}_{0.2}\text{S}_{0.8}$	$4.230 \pm 0.001$	$6.931 \pm 0.001$	$7.867 \pm 0.003$	$99.656 \pm 0.007$	5.12
$\text{Ag}_2\text{Ge}_{0.3}\text{S}_{0.7}$	$4.224 \pm 0.002$	$6.924 \pm 0.002$	$7.852 \pm 0.005$	$99.692 \pm 0.013$	13.09

### 2.3. Thermoelectric Properties

In order to evaluate and measure the thermoelectric parameters ( $\alpha$ ,  $\sigma$ , PF) of the  $\text{Ag}_2\text{S}$ -based samples, we utilized rod-shaped samples with a diameter of 4 mm that were fabricated using cold extrusion from annealed powders.

According to the results presented in Figure 6 and Table 3, the absolute value of the Seebeck coefficient decreased as the Ge content of the samples increased. The determined negative value of pure  $\alpha\text{-Ag}_2\text{S}$  is  $\alpha = -1051 \mu\text{V}\cdot\text{K}^{-1}$ .

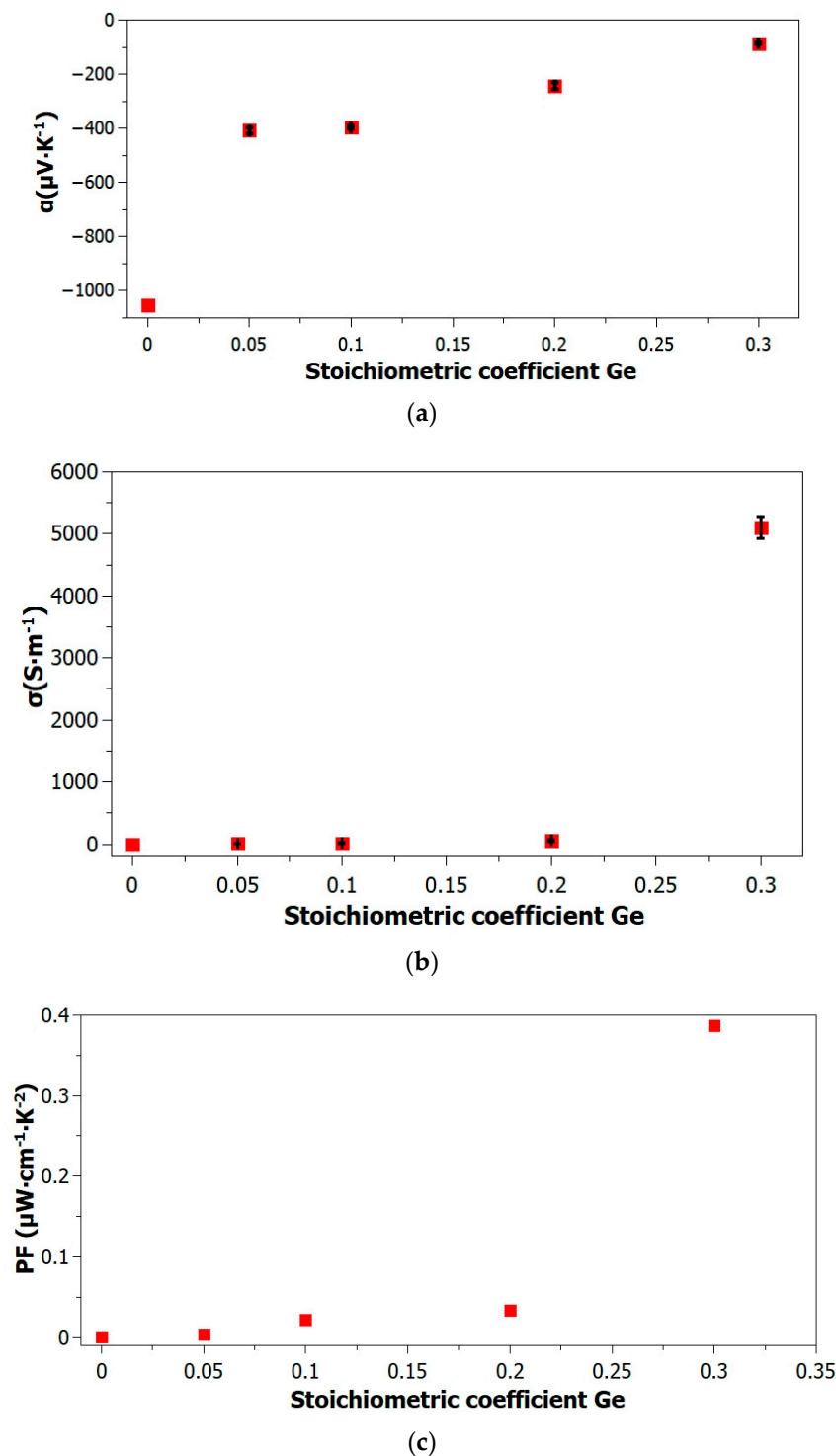


**Figure 6.** Thermoelectric parameters vs. Ge content in  $\alpha\text{-Ag}_2\text{S}$ -based samples: (a) Seebeck coefficient, (b) electrical conductivity  $\sigma$ , (c) power factor (PF), the black symbols represent error bars.

**Table 3.** Thermoelectric properties of the  $\alpha$ -Ag<sub>2</sub>S based samples.

	Ag <sub>2</sub> S	Ag <sub>2</sub> Ge <sub>0.05</sub> S <sub>0.95</sub>	Ag <sub>2</sub> Ge <sub>0.1</sub> S <sub>0.9</sub>	Ag <sub>2</sub> Ge <sub>0.2</sub> S <sub>0.8</sub>	Ag <sub>2</sub> Ge <sub>0.3</sub> S <sub>0.7</sub>
$\sigma$ [S·m <sup>-1</sup> ]	0.102	2.3 ± 0.6	14.2 ± 6	58.2 ± 16.5	5106.2 ± 172
$\alpha$ [μV·K <sup>-1</sup> ]	-1051	-408 ± 10	-397 ± 5	-243 ± 12	-87 ± 4
PF [μW·cm <sup>-1</sup> ·K <sup>-2</sup> ]	0.0011	0.0039	0.0224	0.0343	0.3873

According to the electrical conductivity measurements (Figure 6, Table 3), an increase in the Ge content of the samples results in a related increase in electrical conductivity. The absolute value of  $\alpha$ -Ag<sub>2</sub>S in pure form is 0.102 S·m<sup>-1</sup>. The electrical conductivity value provided for each composition is the average of five measurements. Table 4 presents a summary of the materials of Ag<sub>2</sub>S-based doped Se and Te in various stoichiometric compositions.

**Table 4.** Thermoelectrical properties of Ag<sub>2</sub>S-based materials; T<sub>C</sub> represents the phase-transition temperature of composition [25,45].

Material	T <sub>C</sub> [°C]	ZT	PF [μW·cm <sup>-1</sup> ·K <sup>-2</sup> ]
Ag <sub>2</sub> S	177	6.3 × 10 <sup>-5</sup>	0.0011
Ag <sub>2</sub> S <sub>0.9</sub> Se <sub>0.1</sub>	147	7.6 × 10 <sup>-4</sup>	0.013
Ag <sub>2</sub> S <sub>0.7</sub> Se <sub>0.3</sub>	109	0.075	1.08
Ag <sub>2</sub> S <sub>0.5</sub> Se <sub>0.5</sub>	82	0.26	4.84
Ag <sub>2</sub> S <sub>0.4</sub> Se <sub>0.6</sub>	350	1.08	21.45
Ag <sub>2</sub> S <sub>0.8</sub> Te <sub>0.2</sub>	-	0.25	5.3
Ag <sub>2</sub> S <sub>0.5</sub> Se <sub>0.45</sub> Te <sub>0.05</sub>	57	0.44	4.96

According to the PF values (Figure 6, Table 3), an increase in the Ge concentration in the samples results in a related rise in PF. PF is presented at its maximal value for the sample containing the largest quantity of Ge-Ag<sub>2</sub>Ge<sub>0.3</sub>S<sub>0.7</sub>. The PF values of characterized thermoelectric materials, including clathrates (PF<sub>MIN</sub> = 1.5 μW·cm<sup>-1</sup>·K<sup>-2</sup>), Zintl phases (PF<sub>MIN</sub> = 1.3 μW·cm<sup>-1</sup>·K<sup>-2</sup>), and polymer material PEDOT:PSS (PF<sub>MIN</sub> = 0.01 μW·cm<sup>-1</sup>·K<sup>-2</sup>), are comparable to those of the samples under investigation [8,46]. As a result, it is expected that the recently developed thermoelectric material Ag<sub>2</sub>Ge<sub>0.3</sub>S<sub>0.7</sub> will serve as an acceptable option for implementation in thermoelectric devices.

#### 2.4. Mechanical Properties and Hardness

We selected the density, elastic modulus, microhardness, and nanohardness of Ag<sub>2</sub>S-based materials for determination in order to characterize their mechanical properties and hardness. An increase in dopant concentration resulted in a stronger Ag<sub>2</sub>S-based material. Table 5 indicates that the density of the material with the highest doping is 0.13 g·cm<sup>-3</sup>. The maximal deformation of the samples (compression-induced shrinkage) was 30% of the initial height of the test body, as determined by the uniaxial compression test. Ag<sub>2</sub>Ge<sub>0.3</sub>S<sub>0.7</sub> showed the greatest variation in yield strength among the materials listed in Table 5. By reducing the yield strength of a material, Ge enhances its resistance to the external compression of the sample.

The Ge content of materials influences their hardness. The microhardness of the thermoelectric materials decreases as the dopant (Ge) content increases, as measured by the Vickers indenter HV 0.1 (Table 5). The microhardness value of the purified Ag<sub>2</sub>S sample is nearly identical to that of the sample containing the greatest amount of dopant (Table 4). The investigated Ag<sub>2</sub>S-based materials had a higher microhardness than other frequently used thermoelectric materials, such as PbTe (HV = 0.41 MPa), half-Heusler alloys (HV = 9.1–12.8 MPa), and Mg<sub>2</sub>Se (HV = 5.3 MPa) [42,47].

**Table 5.** Mechanical properties of Ag<sub>2</sub>S-based materials.

	Ag <sub>2</sub> S	Ag <sub>2</sub> Ge <sub>0.05</sub> S <sub>0.95</sub>	Ag <sub>2</sub> Ge <sub>0.1</sub> S <sub>0.9</sub>	Ag <sub>2</sub> Ge <sub>0.2</sub> S <sub>0.8</sub>	Ag <sub>2</sub> Ge <sub>0.3</sub> S <sub>0.7</sub>
$\rho$ [g·cm <sup>-3</sup> ]	7.22	7.24	7.26	7.39	7.35
R <sub>p0,2</sub> [MPa]	122	84	73	91	71
HV 0.1	36	32	26	26	34
H <sub>IT</sub> [GPa]	0.5 ± 0.04	0.8 ± 0.02	0.4 ± 0.05	0.4 ± 0.01	0.9 ± 0.02
E <sub>IT</sub> [GPa]	24 ± 1	30 ± 1	22 ± 2	18 ± 2	47 ± 6

The increased microhardness of this material can be ascribed to the substantial quantity of unmelted Ge particles, which lacked adequate homogenization within the powder mixture (see Figure 7a), where a  $d_1$  and  $d_2$  are diagonals. Pure Ge is classified as one of the hardest elements on the Mohs hardness scale, possessing a hardness of 6. Conversely, S and Ag hold lesser positions on the same scale. Nevertheless, microhardness measurements revealed regions of the sample surfaces that were harder than the Ag<sub>2</sub>S matrix. Consequently, we decided to measure the nanohardness using the Berkovich indenter HV<sub>IT</sub>. Figure 7b, which shows the nanohardness measurement, demonstrates that the sample was not homogeneous, as the boundaries of the matrix and Ge particles are evident.

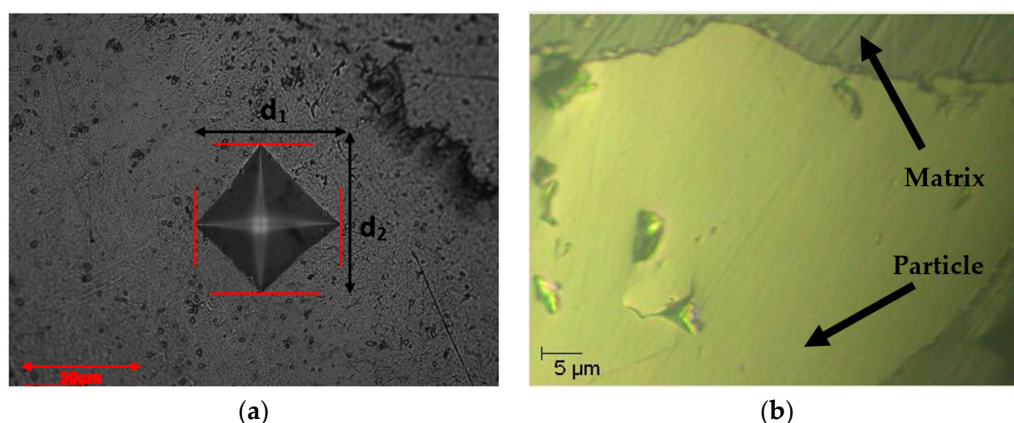


**Figure 7.** (a) Vickers indenter applied in the matrix of Ag<sub>2</sub>S; (b) particle of Ag<sub>2</sub>Ge<sub>0.05</sub>S<sub>0.95</sub> incorporated via Berkovich indenter.

The highest force that could be applied to Ag<sub>2</sub>Ge<sub>0.3</sub>S<sub>0.7</sub> was 47 GPa. When comparing Ag<sub>2</sub>S to the most doped material, the force applied to Ag<sub>2</sub>S was double. Therefore, the mechanical properties of the samples are improved by the addition of Ge.

The results of the present investigation indicate that the Ag<sub>2</sub>Ge<sub>0.3</sub>S<sub>0.7</sub> material shows improved ductility and resistance to mechanical damage, making it viable for application in thermoelectrical devices that are susceptible to mechanical strain (see Table 5).

### 3. Discussion

Ag<sub>2</sub>S that has been doped shows potential as a thermoelectric material. Five samples containing different concentrations of Ge were produced, utilizing the previously mentioned techniques. The chemical composition was verified by means of SEM EDX analysis. The observed values of the components were virtually equivalent to the expected values. It is obvious from the initial Ag and S mapping that the matrix includes regions that are absent (darker). We determined, using EDX analysis, that these regions represent Ge particles that were too large to be incorporated into the structure of the matrix. In order to achieve a more seamless integration into the structure, it becomes essential to consider alternative homogenization techniques.

The addition of Ge causes an increase in the matrix parameter. The correlation between the measured values and the expected values obtained from the COD database

was validated by X-ray diffraction. The sample with the greatest amount of Ge showed a measurement error of 13.09% (Rw). The possible cause of this error is an excessive quantity of additive doping that failed to be fully integrated into the  $\text{Ag}_2\text{S}$  structure, as indicated in Table 2. It is clear that  $\text{Ag}_2\text{Ge}_{0.3}\text{S}_{0.7}$  is a two-phase compound due to inadequate Ge incorporation. As the quantity of doping increases, so do the thermoelectric parameters. From that point forward, the absolute value of the Seebeck coefficient fell by two orders. Conversely, the electrical conductivity exhibited a fourfold increase in comparison to pure  $\text{Ag}_2\text{S}$ . The Seebeck coefficient of  $\text{Ag}_2\text{Ge}_{0.3}\text{S}_{0.7}$  indicates that as the amount of dopant increased, we approached the N-P-type transition.

The elastic modulus exhibited a range of 18–47 GPa. Between 0 and 0.1 atomic percent Ge, the value of the elastic modulus increased and then decreased; as the amount of Ge increased, the most doped sample achieved its maximum value.

The influence of doping is obvious from the hardness and individual mechanical property measurements. The mechanical properties of the thermoelectric material have been significantly improved as a result of doping. The yield strength decreased from 122 MPa to 71 MPa. Materials doped with Ge exhibit enhanced elasticity, as indicated by the rise in elastic modulus (Table 5).

The microhardness values showed variability, rising from 0.9 GPa to 0.4 GPa, with no discernible correlation. In order to improve the characterization of the mechanical properties of  $\text{Ag}_2\text{S}$ -based materials, hardness measurements are indispensable. Hardness could be used to classify the material in its entirety, encompassing its heterogeneous elements.

The endeavor to enhance the properties of Ge by increasing its quantity encounters formidable challenges, primarily attributed to the incomplete integration of Ge within the crystalline lattice. In response to this predicament, we acknowledge the imperative to explore alternative synthesis methodologies aimed at achieving full Ge incorporation into the unit cell. While the introduction of Ge has demonstrated notable enhancements in bulk electrical conductivity, it is imperative to acknowledge the potential inadvertent consequence of heightened thermal conductivity. Accordingly, forthcoming research endeavors will be directed towards surmounting these obstacles and devising strategies to optimize the thermoelectric properties of  $\text{Ag}_2\text{S}$ -based materials.

Furthermore, the partial inclusion of Ge within  $\text{Ag}_2\text{S}$ -based materials engenders notable advancements in mechanical and thermoelectric performance. The impact of Ge incorporation on the overall material characteristics underscores the necessity to investigate alternative synthesis techniques that may facilitate complete Ge integration. Noteworthy is the observation that the incorporation of Ge augments the bulk electrical conductivity of the material. However, it is essential to recognize that the concomitant elevation in electrical conductivity may give rise to undesirable increments in thermal conductivity.

#### 4. Materials and Methods

The  $\text{Ag}_2\text{S}$ -based samples were manufactured using pure Ag, S, and Ge powders. Each material possessed a purity level of 99.99%. The following particle mixtures were produced by mixing the pure powders in their respective proportions:  $\text{Ag}_2\text{S}$ ,  $\text{Ag}_2\text{Ge}_{0.05}\text{S}_{0.95}$ ,  $\text{Ag}_2\text{Ge}_{0.1}\text{S}_{0.9}$ ,  $\text{Ag}_2\text{Ge}_{0.2}\text{S}_{0.8}$ , and  $\text{Ag}_2\text{Ge}_{0.3}\text{S}_{0.7}$  (atom. ratio). In determining the doping amounts of the individual samples, it was guaranteed that the amount did not surpass 50% of the overall weight. Then, through a solid-state reaction caused by the melting of sulfur, powder mixtures were annealed for ten hours at 160 °C in a steel container under an argon atmosphere in order to generate homogeneous  $\alpha$ - $\text{Ag}_2\text{S}$ -based powders. The annealing temperature was selected in order to inhibit the generation of  $\beta$ - $\text{Ag}_2\text{S}$  within the particles. Following annealing, the granules were compacted through cold extrusion into compact rods measuring 100 mm in length and 4 mm in diameter. These compacted bulk materials were used in order to determine sample properties and analyze the microstructure.

One sample of pure  $\alpha$ - $\text{Ag}_2\text{S}$  was produced for the purpose of standardization. The reason Ge was chosen as the dopant in  $\alpha$ - $\text{Ag}_2\text{S}$  was due to its classification as a metalloid, and more precisely as a semiconducting element. However, further research is required to

determine the impact of Ge on the properties of  $\alpha$ -Ag<sub>2</sub>S. The objective of our investigation was to modify the thermoelectric characteristics of  $\alpha$ -Ag<sub>2</sub>S through the replacement of S in its unit cell with Ge.

Two scanning electron microscopes (SEM), JSM 7000F JEOL (Japan) and Vega 3 LMU Tescan (Czechia), were utilized to analyze the chemical composition and microstructure of the samples. Prior to each SEM examination, a 10 mm-long section of the cold-extruded rods was cut. These sections were then cold-mounted with a mounting compound to expose their cross-sections, followed by grinding and polishing. Each microscope was equipped with an EDX analyzer to measure elemental energy dispersive X-rays. The Tescan Vega 3 LMU was used for elemental composition mapping via EDX, while the JEOL JSM 7000F was employed to validate the chemical composition.

In order to discover the phase composition and unit cell parameters of  $\alpha$ -Ag<sub>2</sub>S in powder samples that were not compact, X-ray diffraction was applied. A X-Pert Pro diffractometer Philips (Amsterdam, The Netherlands) was used with a Cu X-ray tube and a value of  $\lambda = 1.5418 \text{ \AA}$ .

The Seebeck coefficient of the 10 mm rods was measured using a device developed in-house. The Keithley 2100/230-240 MULTIMETER served as the potential measuring instrument. Type K thermocouples were employed for temperature measurement, while two Peltier modules were utilized for heating and cooling. Temperature and potential data were collected using brass receptacles (see Figure 8). To ensure stable electrical and thermal contact, the samples were firmly pressed between two brass holders under constant pressure. A hole was created in one brass holder to ensure close contact of the type K thermocouples with the sample, while apertures on the opposing side facilitated cable access for potential measurement. Peltier modules were positioned at both ends of the apparatus to establish a temperature gradient. Electrical conductivity was measured using the same setup, with minor changes. Peltier modules were turned on and additional steel needle spring-loaded probes were pressed against the sample. The rest of the wiring used was copper.

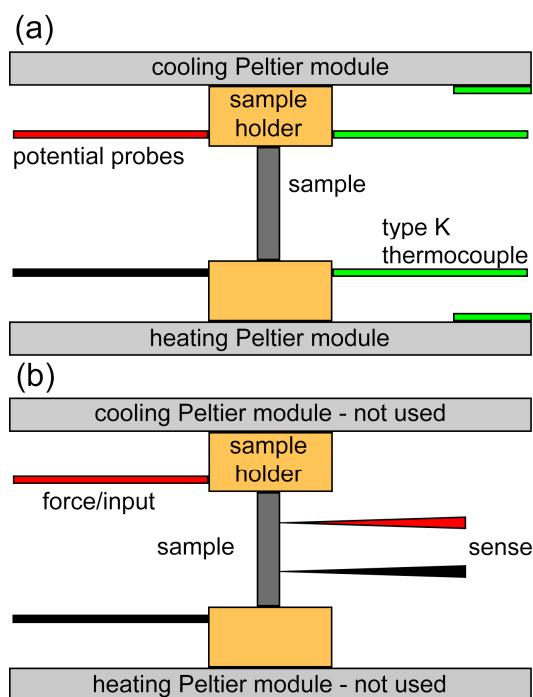


**Figure 8.** Schematic of the apparatus used for (a) Seebeck coefficient and (b) electrical conductivity measurements.

Prior to the measurements, the entire apparatus was calibrated using rods composed of purified elements (Bi, Ni, Sb, and Te) with known Seebeck coefficient values. A 5 °C temperature difference was maintained between the cooled and heated ends of the rod samples, with the cooled end slightly below ambient temperature. Temperature and potential measurements were conducted during the heating, stabilization, and cooling phases. The Seebeck coefficient value was determined by analyzing the temperature difference against the potential for both heating and cooling phases, and a linear function was applied to the data. A linear correction factor, based on the calibration, was then applied. A separate comprehensive explanation and characterization of the apparatus is currently being developed.

Two independent tests were chosen to evaluate the mechanical properties of the prepared samples: the uniaxial compression test and the hardness test.

The purpose of conducting hardness tests, which include both nanohardness and microhardness tests, was to assess the resistance of small samples to plastic deformation induced by a standardized source. The objective of these experiments was to investigate the influence of the dopant on the mechanical properties of the samples.

The methodology employed for measuring the elastic modulus and nanohardness involves depth sensing indentation (DSI) using TTT-NHT testing apparatus (CSM Instruments, Peseux, Switzerland). The tests were conducted in linear mode with a Berkovich pyramid diamond tip. A force of 50 mN was applied to each sample for a duration of 10 s, with loading and unloading processes occurring at a speed of 150 mN/min. The load-penetration depth (P-h) profiles obtained were analyzed following the Oliver and Pharr method [48]. This analysis included the calculation of elastic and plastic deformation energies, as well as the determination of hardness and elastic modulus values as a function of depth. A maximum of 15 indentations were performed, and the resulting data underwent statistical analysis [47,48].

Using a Vickers indenter and a Wilson–Wolper Tukon 1102 microhardness instrument (Esslinger, Germany), the microhardness HV was determined to be 0.1. Each sample was examined a maximum of ten times with a 10-s hold and a 100 mN force.

The purpose of the uniaxial compression tests was to determine the behavior of the samples under crushing stresses. The examinations were performed utilizing a TIRATEST 2300 instrument (TIRA, Schalkau, Germany). Cylindrical test samples with a diameter-to-length ratio of 1:2 were manufactured in accordance with the ASTM-E9-89 standard [49,50].

The length of the analyzed samples was 8 mm, with a diameter of 4 mm. To ensure the reproducibility of the results, a minimum of five samples of each composition were produced for data collection. The compression of the samples occurred at a rate of 0.2 mm/min. The densities of the samples were determined using Archimedes' method, for which each sample was weighed at least five times to ensure accuracy.

## 5. Conclusions

The addition of Ge significantly improves the power factor of materials based on Ag<sub>2</sub>S. Cold extrusion using a hydraulic press is a potentially effective manufacturing technique that yields increased hardness levels. The following material compositions—Ag<sub>2</sub>S, Ag<sub>2</sub>Ge<sub>0.05</sub>S<sub>0.95</sub>, Ag<sub>2</sub>Ge<sub>0.1</sub>S<sub>0.9</sub>, Ag<sub>2</sub>Ge<sub>0.2</sub>S<sub>0.8</sub>, and Ag<sub>2</sub>Ge<sub>0.3</sub>S<sub>0.7</sub>—were manufactured and characterized. The power factor (PF) value of pure Ag<sub>2</sub>S is close to zero. However, Ge doping significantly enhances the electrical conductivity and produces a more positive Seebeck coefficient. Our attempt to create an entirely P-type material for use in thermoelectric homojunctions with minimal dopant quantities failed. The sample containing Ag<sub>2</sub>Ge<sub>0.3</sub>S<sub>0.7</sub> had the highest PF. In subsequent attempts to achieve more efficient dopant–material integration, an alternative homogenization technique should be implemented. The results suggest that the materials created contain two distinct phases, namely, Ag<sub>2</sub>S and unincorporated Ge. As previously established, the basic cell retains its dimensions; furthermore, X-ray diffraction indicates that dopant integration into the structure is only partial. The crystalline character of the Bragg diffraction peaks is consistent with previously available

data. Additionally, SEM EDX confirmed that Ge was not incorporated into the Ag<sub>2</sub>S, but rather dispersed throughout the sample as larger Ge grains. Insufficient dopant integration was achieved through the selected procedure. The results obtained from the measurements clearly indicate that the dopant had an impact on various properties, including mechanical and hardness characteristics, even when present as individual granules of Ge within the structure. Alternative synthesis techniques might be more appropriate for achieving complete Ge incorporation into the unit cell. The incorporation of Ge into the material results in an enhancement of its bulk electrical conductivity. A rise in thermal conductivity, on the other hand, could be an unintended consequence of an increase in electrical conductivity. Doping increases the elasticity and flexibility of the material, which suggests potential applications in the field of ubiquitous electronic devices and sensors. In conclusion, the potential of Ag<sub>2</sub>S-based materials partially doped with Ge to exhibit enhanced mechanical and thermoelectric properties was demonstrated. However, it is evident that the achieved power factor of  $0.38 \mu\text{Wcm}^{-1}\text{K}^{-2}$  falls short of the levels required for practical thermoelectric applications. Future research efforts should focus on optimizing the synthesis method to fully incorporate Ge into the unit cell and exploring strategies to significantly enhance the power factor by at least one order of magnitude. It is essential to consider the trade-off between improving electrical conductivity and minimizing the undesirable increase in thermal conductivity associated with Ge doping.

**Author Contributions:** Conceptualization, G.H., F.M. and K.S.; methodology, R.D., Z.M., B.B., P.L., A.P. and K.S.; investigation, W.M., G.H. and F.M.; data curation, G.H. and F.M.; writing—review and editing, G.H. and F.M. All authors have read and agreed to the published version of the manuscript.

**Funding:** This work was supported by the Slovak Research and Development Agency (contract nos.: APVV-20-0138, APVV-20-0205, and APVV-22-0289); the Scientific Grant Agency of the Ministry of Education, Science, Research and Sport of the Slovak Republic and the Slovak Academy of Sciences (VEGA project no.: 2/0039/22; KEGA project no.: 011TUKE-4/2023); and the Technical University of Kosice (grant number: 05/TUKE/2023). This research was funded in part by the international project EIG CONCERT- Japan/2021/215/EHSAL.

**Data Availability Statement:** The data presented in this study are available upon request from the corresponding author.

**Conflicts of Interest:** The authors declare no conflicts of interest.

## References

1. Lundstrom, M.; Jeong, C. *Near-Equilibrium Transport: Fundamentals and Applications; Lessons from Nanoscience*; World Scientific: Singapore; Hackensack, NJ, USA, 2013; Volume 2.
2. Goldsmid, H.J. *Introduction to Thermoelectricity*; Springer Series in Materials Science; Springer: Berlin/Heidelberg, Germany, 2016; Volume 121. [[CrossRef](#)]
3. Goldsmid, H.J. *The Physics of Thermoelectric Energy Conversion*; IOP Publishing: Bristol, UK, 2017. [[CrossRef](#)]
4. Wei, J.; Yang, L.; Ma, Z.; Song, P.; Zhang, M.; Ma, J.; Yang, F.; Wang, X. Review of current high-ZT thermoelectric materials. *J. Mater. Sci.* **2020**, *55*, 12642–12704. [[CrossRef](#)]
5. Jayathilaka, W.A.D.M.; Qi, K.; Qin, Y.; Chinnappan, A.; Serrano-García, W.; Baskar, C.; Wang, H.; He, J.; Cui, S.; Thomas, S.W.; et al. Significance of Nanomaterials in Wearables: A Review on Wearable Actuators and Sensors. *Adv. Mater.* **2019**, *31*, 1805921. [[CrossRef](#)] [[PubMed](#)]
6. He, R.; Schierning, G.; Nielsch, K. Thermoelectric Devices: A Review of Devices, Architectures, and Contact Optimization. *Adv. Mater. Technol.* **2018**, *3*, 1700256. [[CrossRef](#)]
7. Yang, S.; Qiu, P.; Chen, L.; Shi, X. Recent Developments in Flexible Thermoelectric Devices. *Small Sci.* **2021**, *1*, 2100005. [[CrossRef](#)]
8. Wolf, M.; Hinterding, R.; Feldhoff, A. High Power Factor vs. High zT—A Review of Thermoelectric Materials for High-Temperature Application. *Entropy* **2019**, *21*, 1058. [[CrossRef](#)]
9. Sootsman, J.R.; Chung, D.Y.; Kanatzidis, M.G. New and Old Concepts in Thermoelectric Materials. *Angew. Chem. Int. Ed.* **2009**, *48*, 8616–8639. [[CrossRef](#)]
10. Mitra, M.; Benton, A.; Akhanda, M.S.; Qi, J.; Zebajadi, M.; Singh, D.J.; Poon, S.J. Conventional Half-Heusler alloys advance state-of-the-art thermoelectric properties. *Mater. Today Phys.* **2022**, *28*, 100900. [[CrossRef](#)]
11. Tian, Z.; Lee, S.; Chen, G. Comprehensive review of heat transfer in thermoelectric materials and devices. *Annu. Rev. Heat Transf.* **2014**, *17*, 425–483. [[CrossRef](#)]

12. Riffat, S.B.; Ma, X. Thermoelectrics: A review of present and potential applications. *Appl. Therm. Eng.* **2003**, *23*, 913–935. [[CrossRef](#)]
13. Chen, L.; Liu, R.; Shi, X. General principles of thermoelectric technology. In *Thermoelectric Materials and Devices*; Elsevier: Amsterdam, The Netherlands, 2021; pp. 1–18. [[CrossRef](#)]
14. Dahal, T.; Jie, Q.; Joshi, G.; Chen, S.; Guo, C.; Lan, Y.; Ren, Z. Thermoelectric property enhancement in Yb-doped n-type skutterudites Yb<sub>x</sub>Co<sub>4</sub>Sb<sub>12</sub>. *Acta Mater.* **2014**, *75*, 316–321. [[CrossRef](#)]
15. Bell, L.E. Cooling, Heating, Generating Power, and Recovering Waste Heat with Thermoelectric Systems. *Science* **2008**, *321*, 1457–1461. [[CrossRef](#)] [[PubMed](#)]
16. Zuhud, A.M.; Mochammad, F.; Widayat, W. Thermoelectric application in energy conservation. *E3S Web Conf.* **2018**, *73*, 01009. [[CrossRef](#)]
17. Liu, Z.; Tian, B.; Li, Y.; Guo, Z.; Zhang, Z.; Luo, Z.; Zhao, L.; Lin, Q.; Lee, C.; Jiang, Z. Evolution of Thermoelectric Generators: From Application to Hybridization. *Small* **2023**, *19*, 2304599. [[CrossRef](#)]
18. Lv, H.; Liang, L.; Zhang, Y.; Deng, L.; Chen, Z.; Liu, Z.; Wang, H.; Chen, G. A flexible spring-shaped architecture with optimized thermal design for wearable thermoelectric energy harvesting. *Nano Energy* **2021**, *88*, 106260. [[CrossRef](#)]
19. Luan, W. Recent developments of thermoelectric power generation. *Chin. Sci. Bull.* **2004**, *49*, 1212. [[CrossRef](#)]
20. Demirbas, A. Global Renewable Energy Projections. *Energy Sources Part B Econ. Plan. Policy* **2009**, *4*, 212–224. [[CrossRef](#)]
21. Polozine, A.; Sirotninskaya, S.; Schaeffer, L. History of development of thermoelectric materials for electric power generation and criteria of their quality. *Mater. Res.* **2014**, *17*, 1260–1267. [[CrossRef](#)]
22. Cao, T.; Shi, X.-L.; Chen, Z.-G. Advances in the design and assembly of flexible thermoelectric device. *Prog. Mater. Sci.* **2023**, *131*, 101003. [[CrossRef](#)]
23. Dhass, A.D.; Babu, L.G.; Pradhan, R.; Murthy, G.V.K.; Sreenivasan, M. Energy Harvesting Through Thermoelectric Generators. In *Materials and Technologies for a Green Environment*; Hari Krishnan, S., Ed.; Bentham Science Publishers: Soest, The Netherlands, 2023; pp. 32–66. [[CrossRef](#)]
24. Zhou, W.-X.; Wu, D.; Xie, G.; Chen, K.-Q.; Zhang, G.  $\alpha$ -Ag<sub>2</sub>S: A Ductile Thermoelectric Material with High ZT. *ACS Omega* **2020**, *5*, 5796–5804. [[CrossRef](#)]
25. Zhu, M.; Shi, X.-L.; Wu, H.; Liu, Q.; Chen, Z.-G. Advances in Ag<sub>2</sub>S-based thermoelectrics for wearable electronics: Progress and perspective. *Chem. Eng. J.* **2023**, *473*, 145236. [[CrossRef](#)]
26. Wei, T.; Qiu, P.; Zhao, K.; Shi, X.; Chen, L. Ag<sub>2</sub>Q-Based (Q = S, Se, Te) Silver Chalcogenide Thermoelectric Materials. *Adv. Mater.* **2023**, *35*, 2110236. [[CrossRef](#)] [[PubMed](#)]
27. Shi, X.; Chen, H.; Hao, F.; Liu, R.; Wang, T.; Qiu, P.; Burkhardt, U.; Grin, Y.; Chen, L. Room-temperature ductile inorganic semiconductor. *Nat. Mater.* **2018**, *17*, 421–426. [[CrossRef](#)] [[PubMed](#)]
28. Živković, D.; Sokić, M.; Živković, Ž.; Manasijević, D.; Balanović, L.; Štrbac, N.; Čosović, V.; Boyanov, B. Thermal study and mechanism of Ag<sub>2</sub>S oxidation in air. *J. Therm. Anal. Calorim.* **2013**, *111*, 1173–1176. [[CrossRef](#)]
29. Gusev, A.I.; Sadovnikov, S.I. Acanthite–argentite transformation in nanocrystalline silver sulfide and the Ag<sub>2</sub>S/Ag nanoheterostructure. *Semiconductors* **2016**, *50*, 682–687. [[CrossRef](#)]
30. Liang, J.; Wang, T.; Qiu, P.; Yang, S.; Ming, C.; Chen, H.; Song, Q.; Zhao, K.; Wei, T.R.; Ren, D.; et al. Flexible thermoelectrics: From silver chalcogenides to full-inorganic devices. *Energy Environ. Sci.* **2019**, *12*, 2983–2990. [[CrossRef](#)]
31. Li, L.; Peng, C.; Chen, J.; Ma, Z.; Chen, Y.; Li, S.; Wang, J.; Wang, C. Study the effect of alloying on the phase transition behavior and thermoelectric properties of Ag<sub>2</sub>S. *J. Alloys Compd.* **2021**, *886*, 161241. [[CrossRef](#)]
32. Pal'yanova, G.A.; Chudnenko, K.V.; Zhuravkova, T.V. Thermodynamic properties of solid solutions in the system Ag<sub>2</sub>S–Ag<sub>2</sub>Se. *Thermochim. Acta* **2014**, *575*, 90–96. [[CrossRef](#)]
33. Wang, H.; Ma, H.; Duan, B.; Geng, H.; Zhou, L.; Li, J.; Zhang, X.; Yang, H.; Li, G.; Zhai, P. High-Pressure Rapid Preparation of High-Performance Binary Silver Sulfide Thermoelectric Materials. *ACS Appl. Energy Mater.* **2021**, *4*, 1610–1618. [[CrossRef](#)]
34. Tarachand; Mukherjee, B.; Saxena, M.; Kuo, Y.K.; Okram, G.S.; Dam, S.; Hussain, S.; Lakhani, A.; Deshpande, U.; Shripathi, T. Ag-Nano-inclusion-Induced Enhanced Thermoelectric Properties of Ag<sub>2</sub>S. *ACS Appl. Energy Mater.* **2019**, *2*, 6383–6394. [[CrossRef](#)]
35. Wakhare, S.Y.; Deshpande, M.D. Structural, electronic and optical properties of metalloid element (B, Si, Ge, As, Sb, and Te) doped g-ZnO monolayer: A DFT study. *J. Mol. Graph. Model.* **2020**, *101*, 107753. [[CrossRef](#)]
36. Chen, H.; Shao, C.; Huang, S.; Gao, Z.; Huang, H.; Pan, Z.; Zhao, K.; Qiu, P.; Wei, T.R.; Shi, X. High-Entropy Cubic Pseudo-Ternary Ag<sub>2</sub> (S, Se, Te) Materials With Excellent Ductility and Thermoelectric Performance. *Adv. Energy Mater.* **2023**, *14*, 2303473. [[CrossRef](#)]
37. Singh, J.; Verma, S.S. Global Journal of Researches in Engineering Electrical and Electronics Engineering. *Comp. Fig. Merit Some Common Thermocouples High Temp. Range* **2013**, *11*, 1–7.
38. Chen, L.; Liu, R.; Shi, X. Strategies to optimize thermoelectric performance. In *Thermoelectric Materials and Devices*; Elsevier: Amsterdam, The Netherlands, 2021; pp. 19–50. [[CrossRef](#)]
39. Giri, K.; Wang, Y.-L.; Chen, T.-H.; Chen, C.-H. Challenges and strategies to optimize the figure of merit: Keeping eyes on thermoelectric metamaterials. *Mater. Sci. Semicond. Process.* **2022**, *150*, 106944. [[CrossRef](#)]
40. Tripathi, M.N.; Bhandari, C.M. Material parameters for thermoelectric performance. *Pramana J. Phys.* **2005**, *65*, 469–479. [[CrossRef](#)]
41. Dehkordi, A.M.; Zebajadi, M.; He, J.; Tritt, T.M. Thermoelectric power factor: Enhancement mechanisms and strategies for higher performance thermoelectric materials. *Mater. Sci. Eng. R Rep.* **2015**, *97*, 1–22. [[CrossRef](#)]

42. Guttman, G.M.; Gelbstein, Y. Mechanical Properties of Thermoelectric Materials for Practical Applications. In *Bringing Thermoelectricity into Reality*; Aranguren, P., Ed.; InTech: London, UK, 2018. [[CrossRef](#)]
43. Toby, B.H.; Von Dreele, R.B. *GSAS-II*: The genesis of a modern open-source all purpose crystallography software package. *J. Appl. Crystallogr.* **2013**, *46*, 544–549. [[CrossRef](#)]
44. Gražulis, S.; Daškevič, A.; Merkys, A.; Chateigner, D.; Lutterotti, L.; Quiros, M.; Serebryanaya, N.R.; Moeck, P.; Downs, R.T.; Le Bail, A. Crystallography Open Database (COD): An open-access collection of crystal structures and platform for world-wide collaboration. *Nucleic Acids Res.* **2012**, *40*, D420–D427. [[CrossRef](#)] [[PubMed](#)]
45. Chen, H.; Wei, T.R.; Zhao, K.; Qiu, P.; Chen, L.; He, J.; Shi, X. Room-temperature plastic inorganic semiconductors for flexible and deformable electronics. *InfoMat* **2021**, *3*, 22–35. [[CrossRef](#)]
46. Gayner, C.; Kar, K.K. Recent advances in thermoelectric materials. *Prog. Mater. Sci.* **2016**, *83*, 330–382. [[CrossRef](#)]
47. Qian, L.; Li, M.; Zhou, Z.; Yang, H.; Shi, X. Comparison of nano-indentation hardness to microhardness. *Surf. Coat. Technol.* **2005**, *195*, 264–271. [[CrossRef](#)]
48. Oliver, W.C.; Pharr, G.M. An improved technique for determining hardness and elastic modulus using load and displacement sensing indentation experiments. *J. Mater. Res.* **1992**, *7*, 1564–1583. [[CrossRef](#)]
49. E33 Committee. *Classification for Determination of Single-Number Metrics for Impact Noise*; ASTM International: West Conshohocken, PA, USA, 2021. [[CrossRef](#)]
50. E28 Committee. *Test Methods of Compression Testing of Metallic Materials at Room Temperature*; ASTM International: West Conshohocken, PA, USA, 2022. [[CrossRef](#)]

**Disclaimer/Publisher’s Note:** The statements, opinions and data contained in all publications are solely those of the individual author(s) and contributor(s) and not of MDPI and/or the editor(s). MDPI and/or the editor(s) disclaim responsibility for any injury to people or property resulting from any ideas, methods, instructions or products referred to in the content.